Journal of Molecular Structure 1237 (2021) 130275

Contents lists available at ScienceDirect

Journal of Molecular Structure

journal homepage: www.elsevier.com/locate/molstr

Synthesis, crystallographic, computational and molecular docking studies of new acetophenone-benzoylhydrazones

Temitope A. Ajayeoba[a,*], Joseph O. Woods[b], Ayowole O. Ayeni[a], Tomilola J. Ajayi[d], Raji A. Akeem[b], Eric C. Hosten[c], Olawale F. Akinyele[a]

[a] Department of Chemistry, Obafemi Awolowo University, Ile-Ife 220005, Nigeria
[b] Department of Chemistry, University of Ibadan, Ibadan 200284, Nigeria
[c] Department of Chemistry, Nelson Mandela University, Port Elizabeth 6031, South Africa
[d] Department of Chemistry, Mangosuthu University of Technology, Durban 4000, South Africa

ARTICLE INFO

Article history:
Received 5 November 2020
Revised 15 February 2021
Accepted 8 March 2021
Available online 23 March 2021

Keywords:
Hydrazones
Aldose reductase
DFT
Hirshfeld surface analysis
Molecular docking

ABSTRACT

Three aroylhydrazones, acetophenone-Benzoylhydrazone (I), *p*-hydroxy-acetophenone-benzoylhydrazone (II) and *p*-nitro- acetophenone-benzoylhydrazone (III) have been synthesized and further analyzed with the aid of IR, UV-Vis, and NMR spectroscopic and X-ray Crystallographic techniques. The optimized molecular structures were determined by Density Functional Theory (DFT) using the B3LYP function comprising the 6-311^{++}G (2d, 2p) basis set. The calculated and experimental results for the NMR spectroscopic technique were observed to be consistent. The two reported crystals are monoclinic in the same space group of $P2_{1/c}$. Hirshfeld surface analyses revealed H···H as the most important intermolecular interactions in compounds **II** and **III**. The molecular docking of the compounds against three enzymes - aldose reductase, aldehyde reductase, and β-glucosidase were also carried out where compound **III** displayed the best inhibition of the enzymes with a binding energy of -11.30, -9.58 and -11.10 Kcal mol^{-1} against aldose reductase, aldehyde reductase, and β- glucosidase respectively.

1. Introduction

Aroyl hydrazones are previously reported to show great biological activities, can impact biological processes mediated by enzymes and can serve as polydentate ligands in coordination chemistry in addition to catalytic properties and high thermal stability [1–5]. For example, the use of oxidovanadium metal complexes of hydroxylbenzoylhydrazone for the oxidation of alcohols to ketones with up to 99% efficiency is documented in the literature [6]. The importance of the flavone, hydrazide and hydrazone linkage in suppressing the activity of α- and β- glucosidase which are enzymes involved in carbohydrate metabolism has been well highlighted in the literature, where most of the hydrazone compounds studied inhibited the activity of the enzyme [7]. In addition, aroylhydrazones have high affinity for chelation toward biologically relevant metal ions, such as Mn(II), Fe(II) and Cu(II) [8–10].

Aldehyde reductase (ALR1) and Aldose reductase (ALR2) are two enzymes that have been widely investigated in some complications reported alongside *diabetes mellitus* [11–13]. Furthermore, these enzymes also play a role during the development of disease conditions such as cancer and sepsis [14–16]. Many experimental studies with animals suggested that potent inhibitors of these enzymes could play an important role in preventing complications like cataract and neuropathy that are associated with diabetes [17–19].

A good understanding of the nature of interaction with binding sites and possible mode of attachment via molecular docking is desirable in understanding the mechanism of reactions of drugs with the target sites. The use of Hirshfeld surface analysis involving intermolecular interactions present within a crystal structure can be effectively correlated with data from crystallographic studies as seen in this study [20,21]. Literature search shows that a combination of experimental with computational methods on molecular structure, spectroscopic and docking studies of organic compounds is now widely utilized [22–24]. Therefore, the determination of molecular structures, Hirshfeld surface analysis, spectroscopic studies and molecular docking of three synthesized aroyl hydrazones with diabetic inducing enzymes is the focus of this study.

* Corresponding author.
E-mail address: tajayeoba@oauife.edu.ng (T.A. Ajayeoba).

https://doi.org/10.1016/j.molstruc.2021.130275
0022-2860/

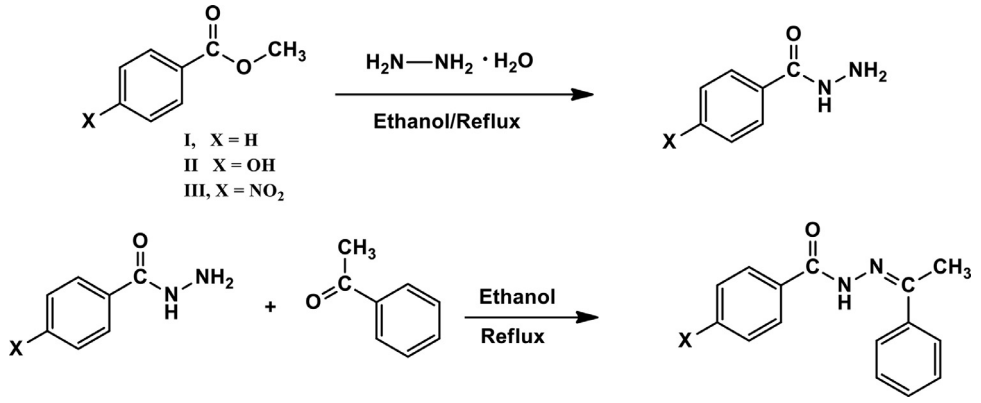

Scheme 1. Synthetic route of the compounds.

2. Experimental section

2.1. Reagents and instruments

Acetophenone, methyl-4-hydroxylbenzoate, methyl-4-nitrobenzoate, ethylbenzoate, hydrazine hydrate solution, were procured from Sigma Aldrich and utilized with no additional purification. ^{1}H and ^{13}C NMR spectra were acquired in d^{6}-DMSO on a 300 MHz Bruker DMX avance spectrophotometer. Fourier transform infrared (FT-IR) spectra for the synthesized compounds within 4000 and 650 cm^{-1} were obtained on a PerkinElmer Spectrum400 spectrophotometer. Electronic spectra in were determined in a solution of ethanol on a Shimadzu UV-Vis 1800 Spectrophotometer.

2.2. X-ray diffraction analysis

Block-shaped, single, white crystals of the hydrazones obtained in an ethanol medium were subjected to X-ray crystallographic analysis. "Bruker KAPPA APEX II single crystal X-ray diffractometer equipped with a 4-circle kappa goniometer and a CCD detector at 295(2) K was used in the collection of crystal data. The instrument consisted of a molybdenum fine focus sealed X-ray tube as an X-ray source and an Oxford cryostream 700 system for sample temperature control [25]. The structure was solved using SHELXT-2014 [26] and refined by least square procedures using SHELXL-2016 [27] with SHELXLE [28] as a graphical interface. Data were recorded for absorption effects using the numerical method implemented in SADABS. All non-hydrogen atoms were refined anisotropically while all hydrogen atoms were refined isotropically. Details on the crystallographic data can be found as supplementary materials in the Cambridge Crystallographic Data Centre (CCDC: 1876117, 1876118). The data can be requested at no cost via www.ccdc.cam.ac.uk/data_request/cif.

2.3. Theoretical calculations

Gaussian 09, revision B01 was utilized to carry out all electronic structure calculations. Structural optimization was done via a "mixed basis set at unrestricted UB3LYP/GENECP level of theory". The B3LYP level and 6-311^{++}G (2d, 2p) basis set were utilized with the atoms in the compounds. "In the process of the DFT calculations, energy values of frontier orbital were determined using the most stable conformation of the reported compounds. NMR shielding constants were predicted using the Gauge-Including Atomic Orbitals - DFT method (GIAO–DFT) in the gaseous and deuterated dimethyl sulfoxide (DMSO) medium" [29,30]. "The 6-311^{++}G (2d, 2p) basis set was used as this was the most widely used standard in Gaussian to determine isotropic shielding constants of ^{1}H and ^{13}C for TMS (tetramethylsilane) which was used as a reference molecule in the Gaussian setup" [31].

2.4. Molecular docking studies

Studies on molecular docking were performed to gain understanding of the binding orientation and interaction of compounds **I - III** with the selected proteins. FRED from OpenEye software [32,33] was used to perform docking studies. After the generation of chemical structures, energy minimization and optimization were carried out by (PM3) semi-empirical method associated with ChemDraw 3D. The crystallographic structures of β-glucosidase, aldehyde reductase and aldose reductase were retrieved from the universal Protein Data Bank using PDB ID: 2O9R, 3FX4 and 1US0 [34,35]. Structures of the target proteins were then protonated in 3D in the standard geometry using MOPAC 7.0 for the optimization of energy. Co-crystals within each target protein were identified as binding sites and further utilized as default parameters in search of systematic conformations. First, co-crystals were re-docked to optimize the docking protocol which was subsequently used for docking of all the three compounds (crystals). Each compound had 10 poses generated for it to realize the final binding positions. Final poses having the least binding form in Chemguass4 were identified and visualized in the Discovery studio [35].

2.5. Synthesis of hydrazones

An established method according to the literature [36,37] was adopted and involved two steps depicted in Scheme 1. 400 mmol of hydrazine hydrate was stirred with equimolar quantities of methylbenzoate, 4-nitromethylbenzoate and 4-hydroxylmethylbenzoate respectively in 150 mL of ethanol on a water bath and then refluxed for 12 hours. The resultant yellowish solution was concentrated using rotary evaporator to give a white crystalline precipitate of the respective hydrazides. The precipitates formed, were filtered with the aid of a suction pump, washed with 40 % ethanol and allowed to dry over $CaCl_2$ in the desiccator.

The hydrazones were synthesized by stirring equimolar quantities of the hydrazide respectively with acetophenone in 100 mL ethanol and further refluxed for 6 hours. The solvent was allowed to evaporate slowly until white needle-like crystalline precipitates were obtained. These were filtered and washed with 40 % ethanol. The precipitate was air-dried for 20 minutes and then placed in a desiccator over $CaCl_2$.

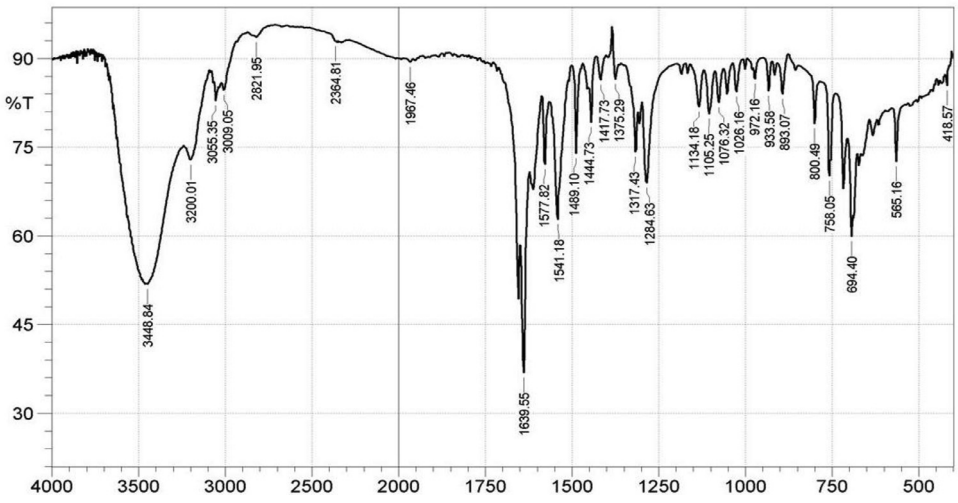

Fig. 1. The experimental IR spectrum of compound **I**.

Table 1
Experimental data (ppm) for the ^{1}H NMR chemical shifts for Compounds **I – III**.

	I	II	III
CH_3	2.39	1.98	2.4
Ar-H	7.43 – 7.89	6.87 – 7.84	7.45 – 8.36
N-H	10.80	10.54	11.10
O-H	-	10.10	-

Table 2
UV-Vis electronic data (nm) for compounds **I - III**.

Compounds	Experimental	
	$\pi \rightarrow \pi^*$	$n \rightarrow \pi^*$
I	225	290
II	220	290
III	250	310

3. Results and discussion

3.1. NMR spectral data

The ^{1}H NMR experimental data for compounds **I – III** are presented in Table 1 while the experimental ^{1}H NMR spectra and ^{1}H/^{13}C theoretical data for all the hydrazones are given in Tables 1a – 1c and Fig. 1 respectively (Supplementary Information). The spectra and calculated data revealed the formation of the compounds, as well as the role played by the *para-* substituents by way of inductive effects. The methyl (CH_3) signal resonated at 2.39 ppm in compound **I**, at 1.98 ppm in **II,** and 2.40 ppm in **III**. The aromatic protons resonated in the range 7.43 -7.89 ppm in **I**, at 7.87-7.84 ppm in **II** and 7.45-8.36 ppm in **III**. The diagnostic N-H signal for hydrazones appeared at 10.80 ppm for the compound **I** while it shifted upfield to 10.58 ppm in **II** and further downfield in **III** to 11.10 ppm as similarly observed in the literature [38,39]. These shifts are the effects of the electron-donating *cum* electron-withdrawing properties impacted by the hydroxyl and the nitro groups on the hydrazones. The signal that appeared at 10.10 ppm in compound **II** was due to the hydroxyl substituent [40].

3.2. *Vibrational* analysis

Fig. 1 presents the experimental FT-IR spectrum of **I** while those of **II** and **III** are in Figs. 2a and 2b (Supplementary Information). The following diagnostic bands "ν(N-H), ν(C=O), ν(C=N) and ν(N-N)" have been identified in the infrared spectra of the hydrazones [33]. The prominently broad band observed at 3200 cm^{-1} in **I** is attributed to ν(N-H) and remained in the same position in **II** but shifted to higher wavenumber at 3265 cm^{-1} in compound **III**.

The ν(C=O) band appeared at 1639 cm^{-1} in **I** and there was a bathochromic shift to lower energy of this bands in **II** to 1620 cm^{-1}. The azomethine ν(C=N) bond resonated at 1577 cm^{-1} and shifted to 1537 cm^{-1} and 1600 cm^{-1} in **II** and **III** respectively. The ν(N-N) vibration showed a similar trend to what was observed in the other bands. The infrared spectra data revealed the inductive effects of the substituents on the system. [41]. In addition, OH stretching frequency was at 3406 cm^{-1} in compound **II** while NO_2 group resonated as two bands observed at 1348 and 1512 cm^{-1} in compound **III**.

3.3. UV-Vis analysis

The experimental data are presented in Table 2 for the three compounds. Two electronic transitions were prominent in the reported UV-Vis spectra of the hydrazones. The band that occurred at 225 nm in **I** is ascribed to the $\pi \rightarrow \pi^*$ and this band underwent hypsochromic shift to higher energy in **II** to 220 nm and bathochromic shift to lower energy in **III** to 250 nm [42].

The second prominent band at 290 nm in **I** and **II** is due to $n \rightarrow \pi^*$ transition and shifted significantly to 310 nm in **III**. This could be attributed to the nitro- substituent on the benzene ring as it had been reported to lead to an increase in the wavelength of absorption in similar compounds [43].

3.4. X-ray *diffraction* data analysis

The ORTEP diagrams of compounds **II** and **III** are presented in Fig. 2 with the crystallographic data of the reported compounds summarized in Table 3 while the packing diagrams are in Fig. 4 (Supplementary Information). Also, the summary of hydrogen bonding interactions is presented in Table 4. The bond parameters of the synthesized compounds showed some similarity with each other, and within normal ranges of similar compounds reported in the literature [44,45]. In the presented compounds, the azomethine (C=N) bond distances are 1.289(18) Å for **II** and 1.291(17) Å for **III**, indicating that they are typical double bonds. The bond distances between atoms C(1) and N(1) [1.3576(18) Å for **II** and 1.352(17) Å for **III**] lie between the values for single and

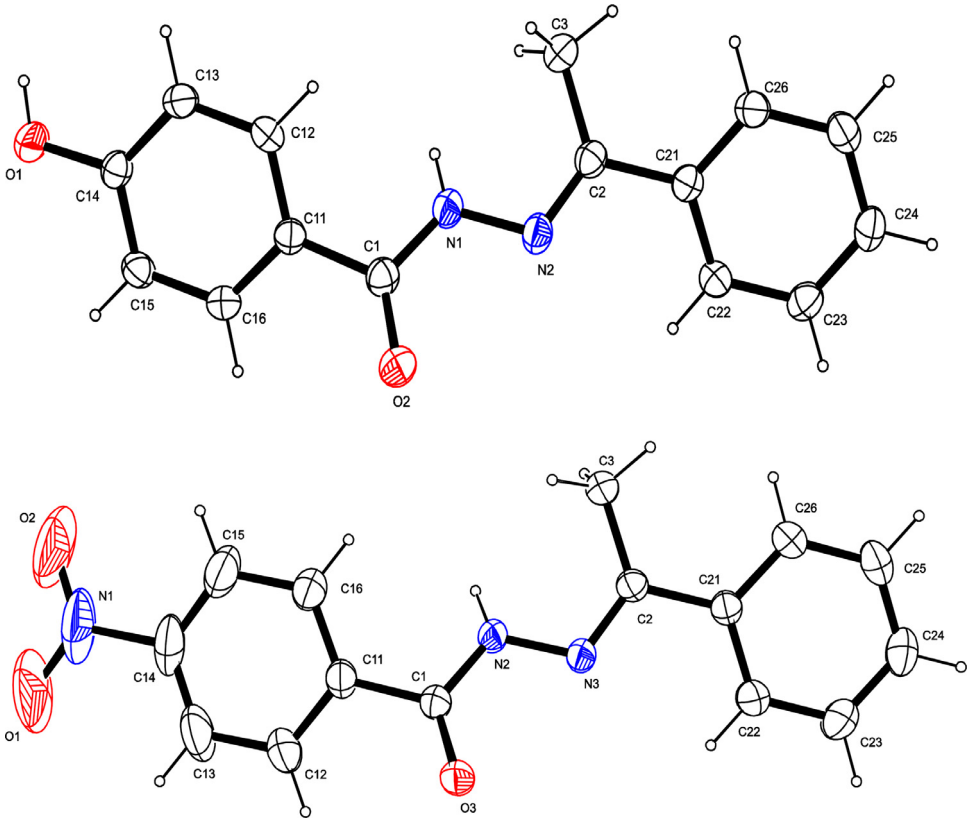

Fig. 2. Molecular Structures of **II** (above) and **III** (below)

Table 3
Crystallographic data for compounds **II** and **III.**

	II	**III**
Formula	$C_{15}H_{14}N_2O_2$	$C_{15}H_{13}N_3O_3$
Formula Weight	254.28	283.28
Crystal System	Monoclinic	Monoclinic
Space group	P 21/n	P 21/c
a/Å	10.9389(8)	5.0414(2)
b/Å	7.3005(4)	32.7645(10)
c/Å	16.2909(12)	8.2176(3)
α/º	90	90
β/º	109.001(3)	93.129(2)
γ/º	90	90
V/Å^3	1230.10(15)	1355.35(8)
Z	4	4
Dcalc/g/cm^3	1.373	1.388
λ(MoKa)(Å)	0.71073	0.71073
F000	536	592
Crystal Size [mm]	0.10 x 0.53 x 0.65	0.07 x 0.23 x 0.77
Temperature (K)	200	200
Theta Min-Max [Deg]	2.0, 28.4	2.5, 28.3
Reflections collected/unique	14130/3084	25740/3377
Final R indices [I > 2s(I)]	R1 = 0.0420, wR2 = 0.1200	R1 = 0.0502,wR2 = 0.1377
Max/min., $\Delta\rho$	0.31/-0.23	0.28/-0.23

Table 4
Distances (Å) and angles (º) involving hydrogen bonds in compounds **II** and **III**.

D-H···A	*d*(D-H)(Å)	*d*(H···A)(Å)	*d*(D···A)(Å)	Angle(*D*-H···A)(º)
II				
O(1)-H(1)···O(2)	0.8500(2)	1.8200(2)	2.6481(14)	167.00(2)
N(1)—H(1A)···O(1)	0.8300(2)	2.5510(16)	3.1514(16)	130.00(13)
C(3)—H(3B) ···O(1)	0.9800	2.5200	3.4407(18)	157.00
III				
N(2)—H(2)···O(3)	0.8600(2)	2.1800(2)	3.0261(14)	166.70(15)
C(3)—H(3A)···N(3)	0.9800	2.4700	3.4181(18)	162.00
C(13)—H(13)···O(1)	0.9500	2.5900	3.3920(4)	143.00
C(26)—H(26)···O(3)	0.9500	2.5600	3.4353(19)	153.00

D= Donor, H= Hydrogen, A= Acceptor

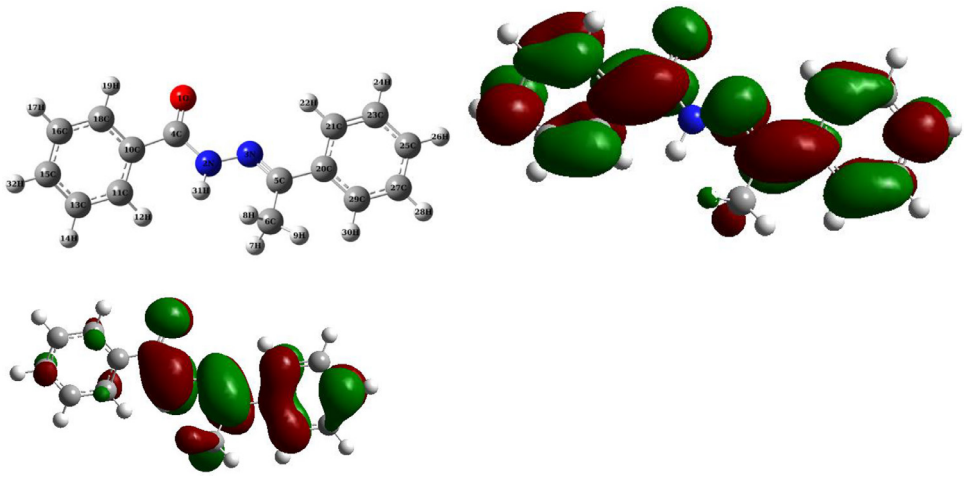

Fig. 3. Optimized geometry, LUMO and HOMO of compounds **I - III**.

Table 5
The global reactivity descriptors (eV) computed of compounds **I - III**.

Parameters (eV)	I	II	III
E_{HOMO}	-0.30604	-0.30388	-0.30659
E_{LUMO}	-0.19557	-0.19071	-0.20065
Energy Bandgap	-0.15034	-0.11317	-0.10594
Ionization potential	0.30604	0.30388	0.30659
Electron affinity	0.19557	0.19071	0.20065
Chemical hardness	0.05524	0.05659	0.05147
Electronegativity	0.25081	0.24730	0.25362
Chemical softness	18.1028	17.6709	19.4288
Chemical potential	- 0.25081	-0.24730	-0.25362
Electrophilicity index	0.5694	0.5403	0.6249

double bonds; this observation is attributed to conjugation effects in the reported compounds [46].

The C–H···O and C–H···N interactions were also observed in addition to the classical inter- and intramolecular N–H···O and N–H···N hydrogen bonds. The oxygen atom also serves as an acceptor for an intra-molecular N–H···O hydrogen bond supported by the amino group of the aminoaroyl moiety as observed in the literature [47]. The stability of crystals of the reported compounds were enhanced by the presence of intermolecular hydrogen bonds and pi···pi stacking. Both compounds have a monoclinic crystal system and the geometric parameters of the molecules agree well with those of similar hydrazones reported in the literature [48,49].

3.5. Theoretical data of the optimized geometry

The determination of properties like HOMO (Highest Occupied Molecular Orbital)) and LUMO (Lowest Unoccupied Molecular Orbital) provided information on the electronic properties of the synthesized compounds [50,51]. Some of the parameters of interest include, “energy band gap” $|E_{HOMO} - E_{LUMO}|$ “ionization potential”, “electron affinity”, “chemical hardness”, “chemical softness”, “electronegativity”, “chemical potential”, “electrophilicity index” and “maximum charge transfer index”. These were evaluated and summarized in Table 5 for the newly synthesized compounds. The optimized geometry and data for compound I are given in Fig. 3 and Table 4a (Supplementary information) respectively.

All the chemical parameters from ionization potential to electrophilicity index were impacted by the inductive effect of the substituent on the aromatic ring and followed a similar trend. For example, the presence of the OH group in compound **II** is seen in its low electrophilicity index due to mesomeric effect involving the hydroxyl group.

3.6. Hirshfeld surface analysis

Fig. 4 presents the diagrams of “inter-contacts by conventional mapping of d_{norm} on molecular HSs”. Short contact areas are depicted in red colour on the Hirshfeld surfaces, while the long distances are indicated blue areas. The most important intermolecular interactions in the form of hydrogen bonds are denoted by red spots and are attributed to the O acceptor atom and H donor. “The large red regions in the d_{norm} surface are also indicative of the probable polymeric nature of the studied compound. The extensions of the molecule represented the donor and acceptor interaction of O-H·····O atoms” [29,52,53]. The red spots indicated areas in which the Oxygen links to the neighbouring complex units through O-H bonds involving the hydroxyl group. The O···H contacts accounted for about 9.4 % of the total interactions that are encountered within the studied system. Pictures of the HS “mapped over shape index (SI)” as well as “curvedness for the studied complex” of the two compounds are presented in Fig. 5 (Supplementary Information). The value of intermolecular distance of interaction between the molecule and its extension is 2.164 and 1.687Å for **II** and 2.038 and 2.038 **Å** in **III** as shown in Fig. 5.

Figs. 6 and 7 contained the 2D plots of the various atom-atom interactions as well as the percentage contributions of the interactions. A significant role is played by the H···H hydrogen bonding interactions within the molecular packing of the studied complex. For **II**, H···H hydrogen bonding interactions accounts for 41.4 % of the whole intermolecular interactions in the studied system and 30.0 %, in **III**. Other interactions include C···H (17 %), N ···H (3 %), C···C (3 %) and H···O (8 %) contacts in **II**, while there were C···H (15 %), N···H (3 %), C···C (3 %) and H···O (13 %) of these contacts in **III**. “All these interaction distances are significantly longer than the van der Waal radii sum of the two elements sharing the interaction” [29,54]. In addition, HS analysis reflects the presence of short H-bonds interactions like C-H…O and C-H...N which are also identified from the crystallographic data.

3.7. Molecular docking results

The binding energies are presented in Table 6 while the binding modes and interaction of all the reported compounds within the active sites of *β-glucosidase* are shown in Table 7. Within the active site of the enzyme, compounds **II** and **III** were found to have high

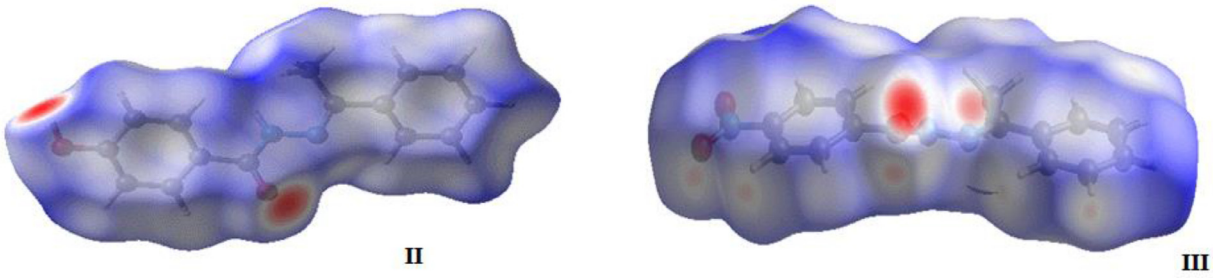

Fig. 4. The Hirshfeld surface of compounds II and III mapped with d_{norm}.

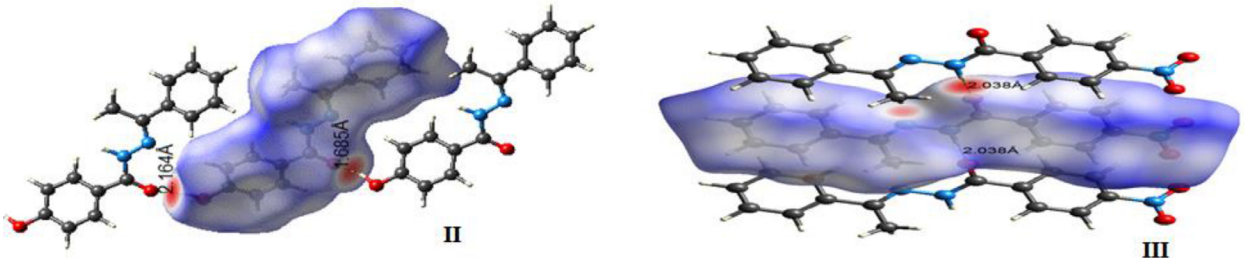

Fig. 5. The intermolecular interaction distance between the donor and acceptor molecules in **II** is 2.164 and 1.687Å and in **III** is 2.038 and 2.038 **Å**

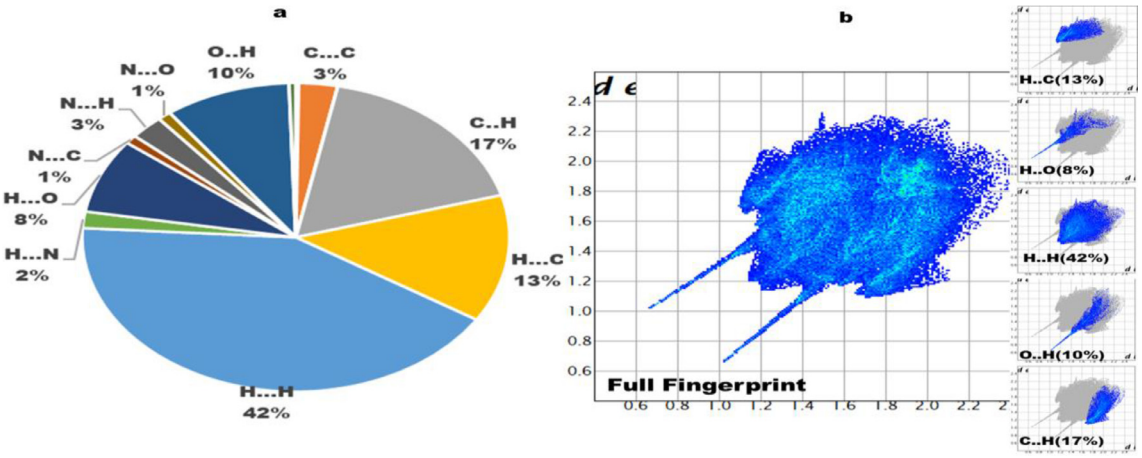

Fig. 6. (a) The summary of intermolecular interactions and their percentages in the crystal structure of **II**. (b)The full and decomposed fingerprint plots of H···H, O···H, H···C, H···O and C···H contacts in compound **II**.

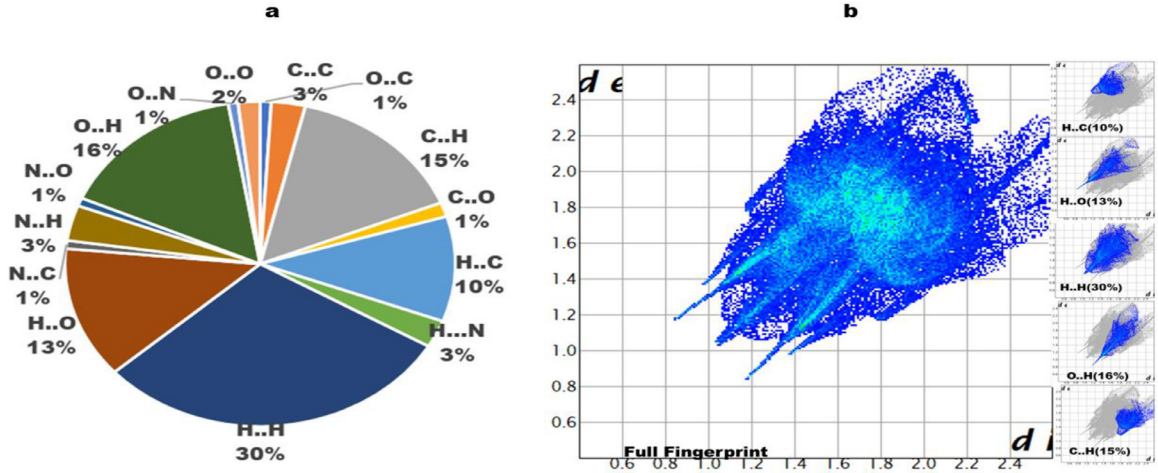

Fig. 7. The summary of intermolecular interactions and their percentages in the crystal structure of **III**. (b)The full and decomposed fingerprint plots of H···H, O···H, H···C, H···O and C···H contacts in compound **III**.

Table 6
ChemGuass4 score of Compounds I - III against target Beta Glucosidase, Aldehyde Reductase and Aldose Reductase Enzymes

Compounds	*Beta Glucosidase (PDB ID: 2O9R)*	*Aldehyde Reductase (PDB ID: 3FX4)*	*Aldose Reductase (PDB ID: 1US0)*
I	-9.790227	-8.240333	-10.811021
II	-11.016876	-8.509027	-10.879704
III	-11.099652	-9.575003	-11.302615

Table 7
Binding Interactions of Compounds I - III with amino acid residues of Respective Target Enzymes

Compounds	*Beta Glucosidase (PDB ID: 2O9R)*	*Aldehyde Reductase (PDB ID: 3FX4)*	*Aldose Reductase (PDB ID: 1US0)*
I	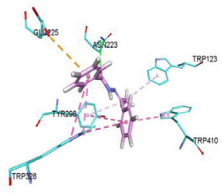	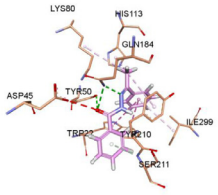	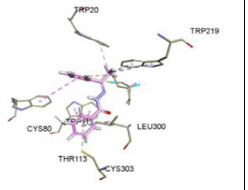
II	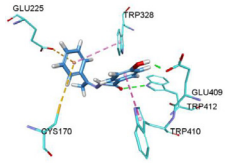	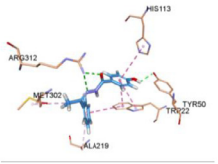	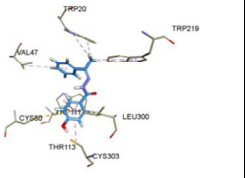
III	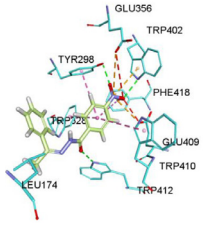	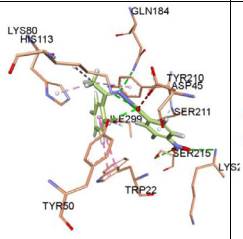	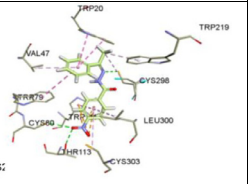

binding energy values of -11.09 Kcalmol^{-1} and -11.02 Kcalmol^{-1} respectively with the enzyme amino acid residues. Compound **I** was found to have a binding energy value (-9.79 Kcal mol^{-1}) which is lower than those of **II** and **III** but fall within the range of values which could be considered moderate for an active inhibitor. The illustration for the binding interaction of the crystals with the active pocket of β-glucosidase enzyme also revealed that amino acid residues such as TRP326, GLU409 and TRP410 are the interacting groups with the hydrazones crystals in the enzyme active pocket. The high binding energy value recorded for **II** and **III** could be accounted for by the increased interaction with the protein due to the presence of hydroxyl and nitro groups which have been linked to an increased binding energy in drug candidates [55,56]. Compound **III** was found to display the highest free binding energy value of -9.58 Kcal mol^{-1} against ALR1. The binding affinity of **I** and **II** were found to be moderate with values of -8.24 Kcal mol^{-1} and -8.51 Kcal mol^{-1} respectively. The major amino acid residues of the enzyme interacting with the compounds were TRP22, TYR50, ARG312 and ASP45.

The results of molecular docking of ALR2 enzyme against the compounds showed that **III** has the highest value (-11.30 Kcal mol^{-1}). The binding affinity of compounds **I** and **II** was very close to the values for **III** (-10.8159 Kcal mol^{-1} and 10.8859 Kcal mol^{-1}) respectively. It is noteworthy to observe that all the compounds interacted closely with the same amino acid residues (LEU300, CYS303, TRP20, VAL47 and THR113) of the enzyme.

4. Conclusion

The syntheses as well as the characterization of three benzoylhydrazones using spectroscopic tools are presented here. The chemical parameters of the hydrazones were further explored using DFT method at B3LYP/ 6-311^{++}G (2d, 2p) level. Intermolecular interactions like H$\cdots$H, C...H, O...H bonding were identified within the crystalline state of the compounds by Hirshfeld Surface Analysis. Molecular docking investigations of the hydrazones against β-glucosidase, ALR1 and ALR2 showed the binding energy and modes of interactions of the compounds inside the enzymes active pockets. The hydrazones generally exhibited high free binding energy towards all the enzymes with the interaction modes of the **III** inside the active site of ALR2 enzyme being the highest, suggesting that it could be further explored in diabetes and its associated conditions.

Declaration of Competing Interest

The authors declare that they have no known competing financial interests or personal relationships that could have appeared to influence the work reported in this paper.

References

[1] M. Ibrahim, R. Sabouni, G.A. Husseini, Curr. Med. Chem. 24 (2017) 193–214.
[2] D.J. Rocca, D. Liu, W. Lin, Acc. Chem. Res. 44 (2011) 957–968.
[3] T.A. Ajayeoba, O.F. Akinyele, A.O. Ayeni, I.J. Olawuni, Am. J. Appl. Chem. 7 (2019) 64–71.
[4] O.F. Akinyele, T.O. Akinnusi, T.A. Ajayeoba, A.O. Ayeni, L.M. Durosinmi, Sci. J. Chem. 7 (3) (2019) 67–71.
[5] S. Anbu, E.C.B.A. Alegria, A.J.L. Pombeiro, Inorg. Chim. Act. 431 (2015) 139–144.
[6] M. Sutradhara, L.M.D.R.S. Martinsa, M. Fátima, G. da S. Armando, J.L. Pombeiroa, Appl. Cat. A: Gen. 493 (2015) 50–57.
[7] I. Syahrul, T. Muhammad, N.H. Ismail, S.M. Kashif, F. Rahim, W. Jamil, M. Hariono, M. Yusuf, W. Habibah, Eur. J. Med. Chem. 103 (2015) 156–170.
[8] A. Ray, S. Banerjee, S. Sen, R. Butcher, G. Rosair, M. Garland, S. Mitra, Struct. Chem. 19 (2007) 209.
[9] J.D. Ranford, J.J. Vittal, Y.M. Wang, Inorg. Chem. 37 (1998) 1226.
[10] P.V. Bernhardt, Dalton Trans (2007) 3214.
[11] T.G. Flynn, N.C. Green, M.B. Bhatia, O. El-Kabbani, Enzym. Mol. Biol. Carbonyl metabolism 372 (2015) 193–194.
[12] N. Das-Evcimen, O. Yildirim, S. Suzen, Arch. Biol. Sc. 61 (2009) 675–681.
[13] A.A. Raji, I.A. Ajayi, S.U. Khan, J. Iqbal, J. Phys. Chem. & Biophy. 7 (2) (2017) DOI, doi:10.4172/2161-0398.1000246.
[14] S.K. Srivastava, K.V. Ramana, A Bhatnagar, Endocrine. Rev. 26 (2005) 380–392.
[15] Y. Lin, Z. Sun, J. Endocrinology 204 (2010) 1–11.
[16] S. Parpart, A. Petrosyan, S.J.A. Shah, A.A. Raji, P. Ehlers, T. Grigoryan, A.F. Mkrtchyan, Z. Mardiyan, A.J. Karapetyan, A.H. Tsaturyan, A. Saghyan, J. Iqbal, P. Langer, RSC Adv. 5 (2015) 107400–107412.
[17] M. Juskova, M. Majekova, V. Demopoulos, M. Stefek, Gen. Physiology Biophysics. 30 (2011) 342–349.
[18] B. Diez-Dacal, F.J. Sanchez-Gomez, P.A. Sanchez-Murcia, I. Milackova, T. Zimmerman, J. Ballekova, E. Garcia-Martin, J.A.G. Agundez, S. Gharbi, F. Gago, S. Milan, D. Perez-Sala, Mol. Pharm. 89 (2016) 42–52.
[19] P. Isorna, J. Polaina, L. Latorre-Garcia, F.J. Canada, B. Gonzalez, J. Sanz-Aparicio, J. Mol. Bol. 371 (2007) 1204–1218.
[20] S. Arshad, R.R. Pillai, D.A. Zainuri, N.C. Khalib, I.A. Razak, S. Armakovic, S.J. Armakovic, C.Y. Panicker, C. Van Alsenoy, J. *Mol. Struct.* 1135 (2017) 234–246.
[21] R.I. Al-Wabli, A.R. Al-Ghamdi, S.V. Aswathy, H.A. Ghabbour, M.H. Al-Agamy, H. Joe, M.I. Atti, Crystals 9 (2017) 1–15.
[22] H. Gökce, Y. Sert, G. Alpaslan, A.S. El-Azab, M.M. Alanazi, M.H.M. Al-Agamy, A.A.M. Abdel-Aziz, ChemistrySelect 4 (2019) 9857–9870.
[23] H. Gökce, Y.B. Alpaslan, C.T. Zeyrek, E. Ağar, A. Güder, N. Özdemir, G. Alpaslan, J. Mol. Struct. 1179 (2019) 205–215.
[24] S. Murugavel, C. Ravikumar, G. Jaabil, P. Alagusundaram, Comput. Biol. Chem. 79 (2019) 73–82.
[25] A.O. Ayeni, G.M. Watkins, E.C. Hosten, J. Mol. Struct. 1160 (2018) 38–45.
[26] G.M. Sheldrick, Acta Crystallogr A71 (2015) 3e8.
[27] G.M. Sheldrick, Acta Crystallogr C71 (2015) 3e8.
[28] C.B. Hubschle, G.M. Sheldrick, B. Dittrich, J. Appl. Cryst. 44 (2011) 1281–1284.
[29] M. Frisch, G. Trucks, H. Schlegel, G. Scuseria, M. Robb, J. Cheeseman, G. Scalmani,V. Barone, B. Mennucci, G. Petersson, G. Wallingford,CT, USA: Gaussian, 2009
[30] T.J. Ajayi, M. Shapi, J. Mol. Struct. 1197 (2019) 308–317.
[31] S.D. Kanmazalp, M. Macit, N. Dege, J. Mol. Struct. 1179 (2019) 181–191.
[32] M. McGann, J. Chem. information and modelling 51 (2011) 578–596.
[33] OEDOCKING 3.2.0.2: OpenEye Scientific Software, Santa Fe, NM. http://www.eyesopen.com, (2017).
[34] E.I. Howard, R. Sanishvili, R.E. Cachau, A. Mitschler, B. Chevrier, P. Barth, V. Lamour, M. Van Zandt, E. Sibley, C. Bon, D. Moras, Proteins: Structure, Function, and Bioinformatics 55 (2004) 792–804.
[35] Accelrys Software Inc., Discovery Studio Modeling Environment, Accelrys Software Inc (2013).
[36] F.A. Adekunle, J.A.O. Woods, O.O.E. Onawumi, A. Odunola, Synthesis and Reactivity in Inorganic, Metal-organic and Nano-metal Chemistry 40 (2010) 430–437.
[37] S. Srinivasan, J. Annaraj, P.R. Athappan, J. Inorg. Biochem. 99 (2005) 876–882.
[38] R. Dinda, P. Sengupta, M. Sutradhar, T.C.W. Mak, S. Ghosh, Inorg. Chem. 47 (2008) 5634–5640.
[39] M. Sutradhar, T. Roy Barman, G. Mukherjee, M.G.B. Drew, S. Ghosh, Polyhedron 34 (2012) 92–101.
[40] S.P. Dash, A.K. Pandab, S. Pasayat, S. Majumder, A. Biswas, W. Kaminsky, S. Mukhopadhyay, S.K. Bhutia, R. Dinda, J. Inorg. Biochem. 144 (2015) 1–12.
[41] A. Eşme, Spec. Lett. (2019), doi:10.1080/00387010.2019.1651339.
[42] T. Ghosh, B. Mondal, T. Ghosh, M. Sutradhar, G. Mukherjee, M.G.B. Drew, Inorg. Chim. Acta 360 (2007) 1753–1761.
[43] D.L. Pavia, G.M. Lampman, G.S. Kriz, J.R. Vyvyan, Introduction to Spectroscopy, Brooks/Cole Cengage Learning, USA, 2009.
[44] Y. Lei, T-Z. Li, C. Fu, X-L. Guan, Y. Tan, J. Chil. Chem. Soc. 60 (2015) 2961–2965.
[45] S.J. Peng, J. Chem. Cryst. 41 (2011) 280–285.
[46] M. Zhang, D-M. Xian, H-H. Li, J-C. Zhang, Z-L. You, *Aust. J. Chem* 65 (2012) 343–350.
[47] M. Çınarlı, C.Y. Ataol, E. Çınarlı, O. İdil, J. Mol. Struct. (2020) doi, doi:10.1016/j.molstruc.2020.128152.
[48] B.P.R. Aradhyula, N. Joshi, K.M. Poluri, M.R. Kollipara, J. Mol. Struct. 1164 (2018) 191–199.
[49] A.B. Salah, A.T. Kandil, M.G. Abd El-Nasser, J. Rad. Res. Appl. Sc. 12 (2019) 413–422.
[50] P. Geerlings, F. De Proft, W. Langenaeker, Chem. Rev. 103 (5) (2003) 1793–1873.
[51] C.G. Zhan, J.A. Nichols, D.A. Dixon, J. Phys. Chem. A 107 (20) (2003) 4184–4195.
[52] M.A. Spackman, D. Jayatilaka, CrystEngComm. 11 (2019) 19–32.
[53] S.K. Wolff, D.J. Grimwood, J.J. Mckinnon, M.J. Turner, D. Jayatilaka, M.A. Spackman, CrystalExplorer (Version 3.1), University of Western Australia, 2012.
[54] A.V. Ivachtchenko, O.D. Mitkin, D.V. Kravchenko, S.M. Kovalenko, S.V. Shishkina, N.D. Bunyatyan, I.S. Konovalova, I.G. Dmitrieva, V.V. Ivanov, T. Langer, Heliyon 5 (2019) e02738.
[55] J.M. Sandes, A.R. Borges, C.G. Junior, F.P. Silva, G.A. Carvalho, G.B. Rocha, R.C. Figueiredo, Bioorg. Chem. 38 (2010) 190–195.
[56] A.C. Anderson, Chem. Biol. 10 (2003) 787–797.